Journal of Applied Polymer Science

WILEY

Applied Polymer SCIENCE

RESEARCH ARTICLE OPEN ACCESS

Linear Viscoelastic Behavior of *n*-Alkane Diluted Polyethylene Melts: Sorption, Desorption, and Oscillatory Rheometry

Ernst Georg Viehböck[1,2] | Georg Gschwendner[3] | Dario Pindrić[1,3] | Gunnar Spiegel[1] | Alexander Hammer[2] | Christian Paulik[1,3] | Gerald Berger-Weber[2]

[1]Competence Center CHASE GmbH, Linz, Austria | [2]Institute of Polymer Processing and Digital Transformation, Johannes Kepler University Linz, Linz, Austria | [3]Institute of Chemical Technology of Organic Materials, Johannes Kepler University Linz, Linz, Austria

Correspondence: Ernst Georg Viehböck (ernst.viehboeck@chasecenter.at)

Received: 18 December 2025 | **Revised:** 8 July 2026 | **Accepted:** 20 July 2026

ABSTRACT

The strategic modification of polymer melt rheology through the incorporation of low-molecular-weight diluents is critical for optimizing industrial processes such as foam extrusion and devolatilization. This study systematically elucidates the influence of a homologous series of *n*-alkanes (C_{10}–C_{18}) on the linear viscoelastic properties of high-density (PE-HD) and linear low-density polyethylene (PE-LLD) melts. To address the experimental challenges posed by volatile components, a rigorous methodological framework was established, integrating gravimetric sorption and desorption kinetics with oscillatory parallel-plate rheometry. Gravimetric analysis substantiated that the diluent mass fraction in the molten state is primarily governed by macromolecular architecture, with the short-chain branched PE-LLD demonstrating a markedly higher sorption capacity than the linear PE-HD due to an enhanced specific free volume. Controlled desorption experiments allowed for the reproducible adjustment of sub-saturation concentrations, where drying kinetics followed a first-order exponential decay. Rheological characterization revealed a pronounced, concentration-dependent reduction in melt viscosity. The application of the Time-Concentration Superposition (TCS) principle enabled the model-independent derivation of horizontal (a_c) and vertical (b_c) shift factors. The established methodology provides a rigorous framework for dilution-assisted rheology modification while outlining clear boundaries for probing future multi-regime scaling transitions.

1 | Introduction

In the realm of polymer engineering, precise rheological control of polymer melts is essential to ensuring stable flow regimes, optimizing energy utilization, and guaranteeing superior product quality [1]. A rigorous route to tailoring melt viscosity involves the incorporation of low-molecular-weight diluents, which can markedly mitigate resistance to flow and thereby expand the processing window [1]. In industrial polyolefin operations, such as high-pressure polymerization, devolatilization loops, and foam extrusion, short-chain hydrocarbon oligomers or volatile blowing agents act as internal diluents that significantly drop melt viscosity and elasticity [1, 2]. Within this framework, *n*-alkanes constitute a scientifically distinctive model system: they are economically viable and form a homologous series chemically identical to the polyethylene backbone. This unique structural identity enables a systematic isolation of pure concentration and molecular-size effects on melt rheology without the confounding factors of chemical incompatibility. Their utilization allows for experimental evaluation under well-defined conditions, offering a unique opportunity to link sorption behavior and viscosity reduction in a robust, fundamental framework.

Consequently, the present work aims to establish a combined experimental–modeling framework that quantifies the viscosity reduction of polyethylene melts induced by *n*-alkane dilution.

Previous works have substantiated that dissolved small molecules, including fluorocarbons and supercritical gasses such as carbon dioxide (CO_2), can significantly reduce the viscosity of polymer melts, with reductions of up to 80% reported for polystyrene/CO_2 systems [3–6]. The magnitude of this reduction is inherently governed by diluent concentration, melt pressure, and the specific polymer–diluent interaction. While the characteristic shape of the shear viscosity curve is typically preserved, the addition of a diluent shifts the entire curve downwards and may alter the onset of shear thinning. Furthermore, extensional viscosity is markedly reduced, which improves processing efficiency and enhances the stretch ratio at break [2, 7].

The mechanisms underlying these phenomena are predominantly attributed to plasticization and dilution. Plasticization arises from an increment in free volume upon the incorporation of diluent molecules, which enhances chain mobility and lowers characteristic transition temperatures such as the glass transition temperature T_g. This effect has been confirmed, for instance, in polydimethylsiloxane (PDMS)/CO_2 systems, where free-volume contributions dominate the viscosity reduction [3]. Concurrently, a "true dilution" effect causes the viscosity of the mixture to approach an intermediate value between that of the polymer and the solvent. Additionally, diluent molecules may act as lubricants, facilitating chain sliding and flow [2].

A rigorous theoretical framework for quantifying these viscoelastic modifications in binary systems was established by the investigations of Schausberger, Knoglinger, and Kastner [8–11]. Their work elucidated the distinct contributions of short-chain molecules to the relaxation spectrum of entangled polymer melts. By applying the concept of Time-Concentration Superposition (TCS), they demonstrated that the viscoelastic response of diluted systems could be unified into master curves using two independent shift factors. Specifically, they identified a vertical shift factor b_c, governed by the dilution of the entanglement network ($b_c \propto w_P^2$), and a horizontal time-shift factor a_c, which they attributed to the increase in free volume introduced by the chain ends of the low-molecular-weight species. This approach, rooted in the Doolittle free-volume theory, provides a robust physical basis for separating the effects of disentanglement from the acceleration of relaxation times, thereby enabling precise modeling of linear viscoelastic properties in plasticized systems.

Beyond rheological considerations, the sorption and solubility of alkanes in semicrystalline polymers have been studied extensively [12, 13]. For polyethylene, solubility and swelling are governed by temperature, density, and alkane chain length [14–16]. Linear low-density polyethylene (PE-LLD), characterized by lower crystallinity and a higher amorphous fraction, exhibits substantially higher sorption capacity and swelling compared to high-density polyethylene (PE-HD) [17–19]. In general, shorter alkanes demonstrate higher gravimetrical diluent mass fractions after sorption than longer analogs. Under exposure to pentane or hexane at elevated temperatures, medium- and low-density PE grades have exhibited critical tipping points that lead to abrupt increases in swelling and, in certain cases, irreversible gel formation [20]. Such phenomena underscore the decisive role of crystallinity and morphology in governing diluent uptake.

Experimentally, the characterization of polymer–diluent systems remains challenging. Conventional rheometers are frequently rendered inadequate because diluent concentrations cannot be maintained under ambient pressure, and bubble nucleation must be strictly avoided. Consequently, specifically modified devices, such as high-pressure capillary and slit-die rheometers, twin-piston viscometers, and in-line rheometry systems, have been developed to mitigate these issues [4, 6, 21–23]. Gravimetric sorption cells and pressure-decay methods are likewise employed to determine equilibrium solubility and diffusion kinetics [24]. These tools are indispensable for establishing reliable structure–property relations in polymer–diluent systems.

Although polymer–gas and polymer–solvent systems have been extensively characterized, systematic investigations of polyethylene melts diluted with homologous *n*-alkanes remain limited. Moreover, predictive models capable of describing viscosity as a continuous function of shear rate, temperature, and diluent concentration are not yet widely available for these specific systems. This study addresses these gaps by integrating controlled sorption and rheological experiments with the superposition principles established by Schausberger and Knoglinger [8, 9]. The resulting framework enables a consistent description and prediction of concentration-dependent viscosity reduction, thereby providing a practical basis for process modeling and rheological tuning in polyethylene–alkane systems and related polymer–solvent solutions.

2 | Experimental

2.1 | Materials

Two commercial polyethylene grades were investigated: a high-density polyethylene (PE-HD, BB2581) and a linear low-density polyethylene (PE-LLD, Borstar FB2230).

The PE-HD grade BB2581 (Borealis GmbH, Vienna, Austria), primarily intended for blow molding, exhibits high stiffness and resistance to environmental stress cracking. According to the supplier's datasheet, it has a density of 0.958 g cm^3 and a melt flow index (MFI) of 0.3 g/10 min (190°C, 2.16 kg). The PE-LLD grade FB2230 (Borealis GmbH) is designed for extrusion processes that require draw-down stability, with a density of 0.923 g cm^3 and an MFI of 0.95 g/10 min (190°C, 5 kg).

Crystallinity values (Table 1) were obtained from differential scanning calorimetry (DSC) with a reference specific energy of a pure PE crystal of 293 Jg^{-1} according to Kong et al. [25].

To investigate dilution effects, five linear *n*-alkanes from *n*-decane to *n*-octadecane were selected as model diluents. These

TABLE 1 | Results of the DSC measurements.

Material	Crystallinity/%
PE-HD	69.6 ± 3.4
PE-LLD	39.5 ± 1.3

TABLE 2 | Overview of the *n*-alkane diluents used in this study.

Chemical	Abbreviation	Supplier	Purity
n-decane	C10	Sigma-Aldrich	>99%
n-dodecane	C12	Sigma-Aldrich	>99%
n-tetradecane	C14	Sigma-Aldrich	>99%
n-hexadecane	C16	Merck	>99%
n-octadecane	C18	Sigma-Aldrich	99%

compounds form a homologous series of non-polar solvents with chemical similarity to the polyethylene backbone. Their abbreviations, suppliers, and purities are listed in Table 2, and thermophysical reference data for C_9–C_{20} alkanes are summarized in Table 3. To provide a clear visual baseline of the homologous diluent series, these established literature reference property trends are illustrated in Figure 1. The pronounced dependence of these thermodynamic quantities on molecular weight highlights the potential for evaporative losses for shorter alkanes when experiments are conducted near their respective boiling points. This tendency decreases with increasing chain length. Furthermore, the increase

TABLE 3 | Physical properties of linear *n*-alkanes (C_9–C_{20}) [26].

Name	C atoms	Molecular weight/g mol^{-1}	Melting point/°C	Boiling point/°C	Density/ kg m^{-3}	Viscosity/ mPa s	Solb. parameter δ/MPa$^{1/2}$
Nonane	9	128.26	−54	151	0.720	0.713	15.6
Decane	10	142.28	−30	174	0.730	0.928	15.8
Undecane	11	156.31	−26	196	0.740	1.186	15.9
Dodecane	12	170.34	−10	216	0.750	1.508	16.0
Tridecane	13	184.37	−5	235	0.756	1.883	16.1
Tetradecane	14	198.39	6	254	0.765	2.131	16.2
Pentadecane	15	212.42	9	270	0.770	2.370	16.3
Hexadecane	16	226.45	18	287	0.777	2.814	16.4
Heptadecane	17	240.47	21	302	0.779	3.591	16.4
Octadecane	18	254.50	28	317	0.800	—	16.5
Nonadecane	19	268.53	30	330	0.786	—	16.5
Eicosane	20	282.55	37	343	0.789	—	16.6

Note: Density, viscosity, and Hildebrand solubility parameter (δ) at 25°C [27].

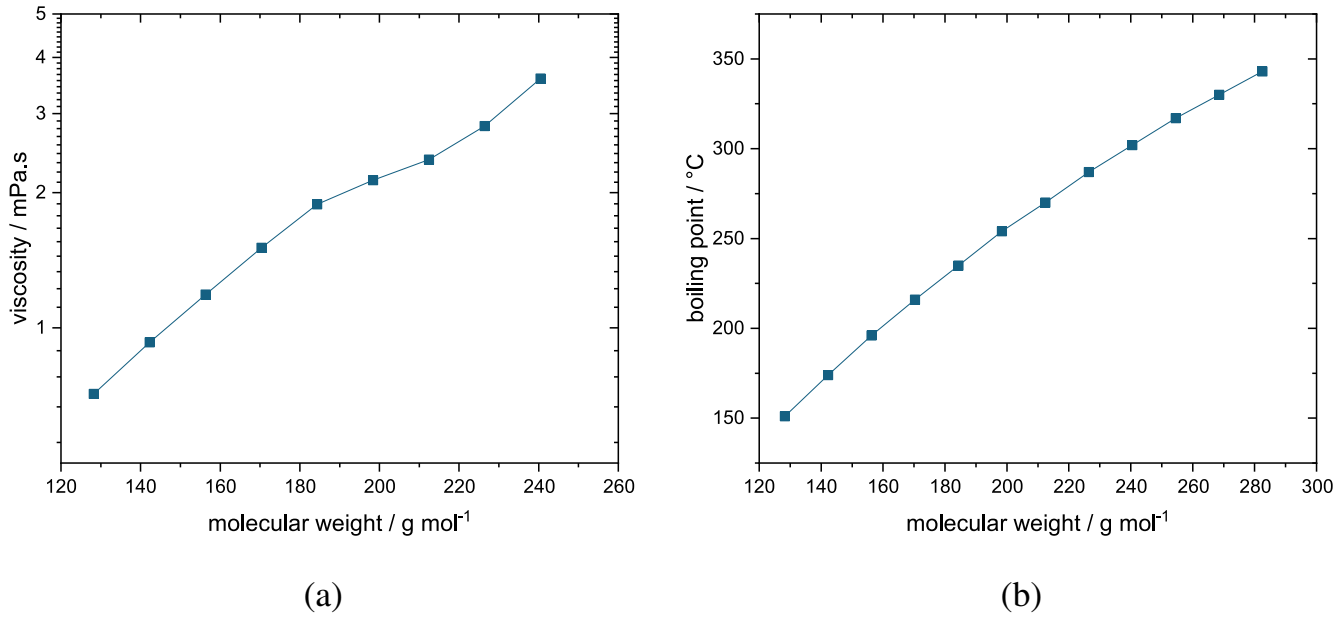

FIGURE 1 | Systematic trends in literature reference data for the linear *n*-alkane series: (a) dynamic viscosity at 25°C and (b) boiling point as functions of molecular weight (compiled from reference data in Table 3). [Color figure can be viewed at wileyonlinelibrary.com]

in viscosity indicates that the effectiveness of viscosity reduction varies systematically with the chain length of the diluent.

2.2 | Sample Preparation and Rheometry

The experimental methodology was structured into a comprehensive four-stage sequence designed to ensure reproducibility and precise control over diluent content. This sequence encompassed specimen fabrication, saturation via high-temperature sorption, controlled desorption to target specific concentrations, and subsequent rheological characterization. Initial specimen fabrication was performed using a hydraulic laboratory hot press (Graseby Specac, Specac Ltd., UK). To obtain homogeneous polymer substrates, the raw material was compression-molded into disc-shaped specimens with a diameter of 25 mm. This process was conducted at a melt temperature of 180°C for PE-HD and 150°C for PE-LLD under a compressive load of 10 t. Immediately following the molding phase, the specimens were subjected to rapid quenching via a water-cooling system to freeze the morphology and ensure rigorous dimensional stability.

To incorporate the diluent into the polymer matrix, the molded discs were subjected to a defined sorption protocol. A custom-engineered stainless steel sorption chamber (sample preparator) was utilized to ensure the complete immersion of the specimens within the respective liquid *n*-alkanes, illustrated in Figure 2. The chamber was hermetically sealed using a chemically resistant gasket and a robust four-bolt clamping mechanism. To maximize the accessible polymer–solvent contact area during sorption, the specimen was positioned atop three minimal, localized protrusions. To establish a rigorous physicochemical basis for the subsequent rheological investigations, the phase state of the binary systems at the characterization temperatures must be explicitly defined. All dynamic mechanical measurements were conducted exclusively in the molten state (150°C for PE-LLD and 180°C for PE-HD), which is above the melting peaks (T_m) of the respective polymers and well below the Lower Critical Solution Temperature (LCST) of polyolefin–alkane systems [13, 14]. In this fully amorphous, isotropic, and molten state, linear *n*-alkanes and polyethylenes exhibit complete thermodynamic miscibility across the entire investigated concentration range, forming a single-phase, homogeneous liquid polymer solution rather than a heterogeneous phase-separated mixture [28].

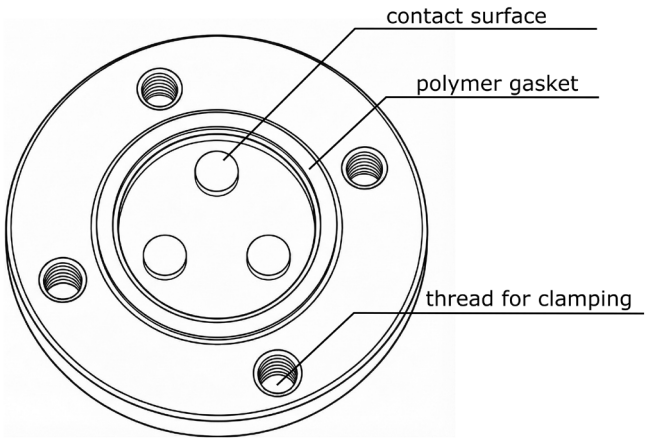

FIGURE 2 | Schematic representation of the custom-engineered sorption chamber employed for specimen saturation. (Illustration generated using Google Gemini).

Subsequent to the saturation phase, the polymer–diluent systems underwent a controlled desorption step to establish discrete sub-saturation concentration levels. This conditioning was carried out in a convection oven (BINDER FD 53, BINDER GmbH, Tuttlingen, Germany) maintained at a constant temperature of 80°C. The samples were conditioned until the specific target weight fractions were achieved, as confirmed by gravimetric analysis.

Finally, the linear viscoelastic properties of the prepared solutions were characterized using a modular compact rheometer (MCR 302, Anton Paar GmbH, Graz, Austria). Measurements were performed using a parallel-plate geometry with a diameter of 25 mm and a measuring gap set to 0.95 mm. Frequency sweeps covering a range from 0.628 rad s^{-1} to 628 rad s^{-1} were executed under a continuous inert nitrogen purge to strictly suppress oxidative degradation of the polymer melt during the analysis. Crucially, the chosen characterization temperatures (150°C for PE-LLD and 180°C for PE-HD) reside far above the typical neat crystalline melting points (T_m) of the respective undiluted polymers, which range from 122°C to 126°C for PE-LLD and 126°C to 135°C for PE-HD [29].

Furthermore, as the high concentrations of dissolved linear *n*-alkanes induce a pronounced thermodynamic melting point depression, the actual clearing points of these polymer-diluent solutions are shifted even further downward. Consequently, throughout the entire duration of the dynamic oscillatory sweeps, the macromolecular matrix is maintained in a assumed purely amorphous, isotropic, and fully molten single-phase state.

To establish a definitive reference state for the subsequent evaluation of dilution effects, the linear viscoelastic properties of the neat, undiluted polyethylene melts were systematically characterized. Figure 3 displays the storage modulus (G') and loss modulus (G'') as a function of angular frequency (ω) within the experimental window of 0.628–628 rad s^{-1}.

The baseline curves reflect typical entangled macromolecular melt dynamics. At lower frequencies, the loss modulus dominates ($G'' > G'$), indicative of terminal relaxation behavior, whereas the high-frequency regime exhibits a transition toward the rubbery plateau. The distinctive horizontal and vertical coordinates of the crossover point ($G' = G''$) for each pure matrix establish the specific reference coordinates ($\omega_{x,1}$, $G_{x,1}$) required for the model-independent derivation of the concentration shift factors a_c and b_c via Equation (2).

3 | Derivation of Concentration Shift Factors

The Time-Concentration Superposition (TCS) principle operates on the premise that the viscoelastic dynamics of entangled polymer solutions can be scaled into master curves by separating structural network dilution from accelerated segmental mobility [8, 30]. These core contributions are mathematically isolated via the vertical modulus shift factor (b_c) and the horizontal time shift factor (a_c), respectively.

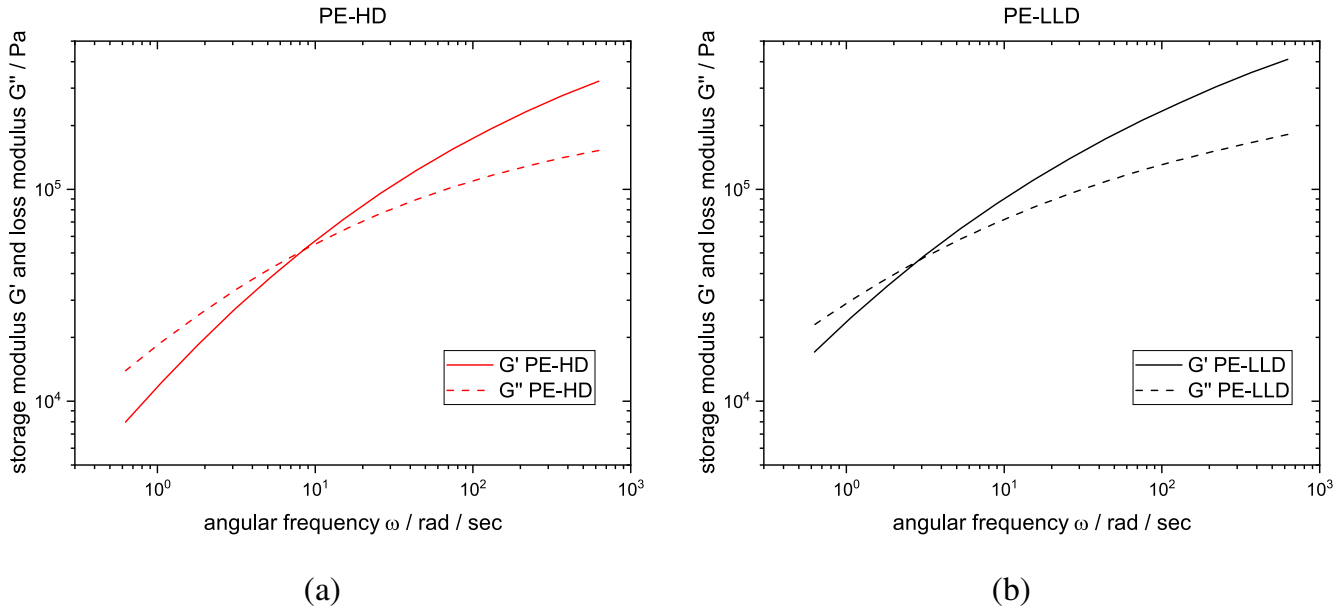

FIGURE 3 | Dynamic frequency sweep spectra of the neat polymer melts serving as the experimental baseline: (a) undiluted PE-HD at 180°C and (b) undiluted PE-LLD at 150°C. Full lines denotes the storage modulus (G'), dashed lines denotes the loss modulus (G''), and the intersection designates the crossover point (COP). [Color figure can be viewed at wileyonlinelibrary.com]

3.1 | Vertical Shift Factor (b_c)

In the concentrated regime, thermodynamic interactions are effectively screened, causing the polymer chains to adopt unperturbed Gaussian dimensions independent of solvent quality [31, 32]. Consequently, the reduction in the plateau modulus (G_N^0) is governed solely by the decrease in the number density of active entanglement strands ($\nu_e \propto 1/M_e$). The vertical shift factor b_c is defined as the normalized ratio of the solution plateau modulus to that of the bulk melt reference [10]:

$$b_c \equiv \frac{G_N^0(\phi)}{G_N^0(1)} \approx w_P^{\alpha} \tag{1}$$

where w_P represents the polymer mass fraction. While binary contact frameworks suggest a quadratic scaling ($\alpha = 2.0$), experimental deviations up to $\alpha = 2.3$ are frequently reported depending on the architectural constraints of the polyolefin matrix [8, 33]. For branched polymers, b_c can sometimes be approximated as unity if the van Gurp Palmen (vGP) plot or the COP trajectory shows a purely horizontal shift upon dilution. For the polymers studied here, however, both the vGP curves and the COP coordinates exhibit a clear vertical component, indicating that b_c deviates measurably from unity and must be retained in the analysis [34]. This structural dilation directly maps to a systematic reduction in the number of entanglements per chain (N_{en}). The subtle influence of the molecular weight distribution (MWD) on this entanglement extraction near saturation boundaries remains an objective for future specialized investigations.

3.2 | Horizontal Shift Factor (a_c)

The horizontal shift factor a_c reflects the kinematic acceleration of the dominant relaxation time (τ_d) upon dilution [10]. Within the tube-model framework, this acceleration is driven by an expanding tube diameter working in tandem with a severe reduction in the monomeric friction coefficient (ζ_0) [32]. In concentrated domains ($w_P \geq 0.35$), the scaling is predominantly governed by the localized enhancement of fractional free volume introduced by the highly mobile diluent chain ends [10, 35].

Crucially, because the solution remains firmly within the highly entangled regime ($N_{en} \gg 1$), this dynamic acceleration is governed by free-volume friction reduction and tube-constraint release rather than a transition to unentangled Rouse modes. A macro-molecular shift toward a Rouse-dominated relaxation regime accompanied by the explicit vanishing of the plateau modulus is expected to occur only at advanced sub-entanglement dilution levels exceeding 65 wt% diluent ($w_P < 0.35$), which lie outside the operational boundaries of this study.

3.3 | Experimental Determination via Crossover Point

While theoretical models provide the physical basis for a_c and b_c, accurate shift factors are experimentally determined in a model-independent manner by superposing the frequency-dependent moduli. An unambiguous reference state for this procedure is the crossover point (COP), defined as the frequency ω_x where the storage modulus equals the loss modulus ($G' = G''$).

Since the shape of the relaxation spectrum is preserved during dilution in the entangled regime, the shift factors can be derived directly from the coordinates of the crossover points of the pure melt ($\omega_{x,1}, G_{x,1}$) and the diluted solution ($\omega_{x,\phi}, G_{x,\phi}$):

$$a_c = \frac{\omega_{x,1}}{\omega_{x,\phi}} \quad \text{and} \quad b_c = \frac{G_{x,\phi}}{G_{x,1}} \tag{2}$$

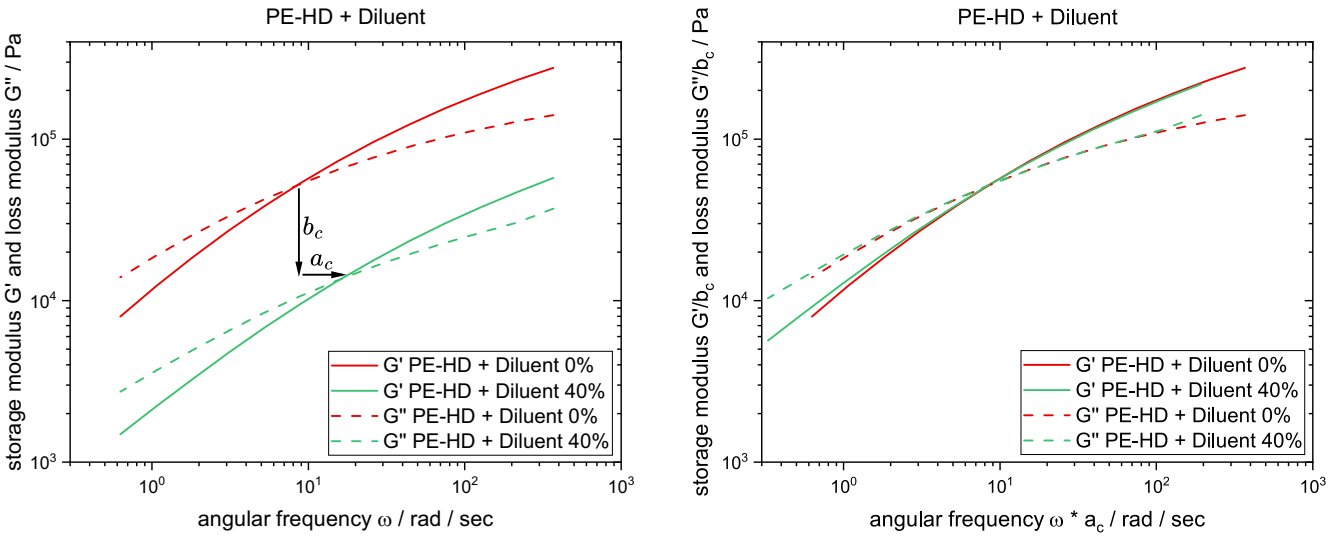

FIGURE 4 | Determination of concentration shift factors via the crossover point (COP) method for a schematic PE-HD/diluent system. (a) Schematic experimental data showing the shift of the COP from the undiluted melt (reference) to the diluted state. The arrows indicate the horizontal shift a_c (time scale) and vertical shift b_c (modulus scale). (b) Master curves constructed via time–concentration superposition, demonstrating superposition of the viscoelastic data. [Color figure can be viewed at wileyonlinelibrary.com]

TABLE 4 | Gravimetrically determined diluent concentrations after 30 min sorption at 150°C.

	PE-LLD		PE-HD	
Diluent	***w*/%**	**STD/%**	***w*/%**	**STD/%**
n-decane	66.5	1.1	62.4	1.1
n-dodecane	66.1	0.7	62.0	0.6
n-tetradecane	65.7	0.7	63.1	0.1
n-hexadecane[a]	62.0	1.5	58.1	2.0
n-octadecane	64.0	0.8	61.0	1.8

[a]Due to the anomalous sorption behavior and elevated standard deviation (STD), solvent contamination was suspected; consequently, *n*-hexadecane was excluded from all subsequent investigations in this study.

here a_c reflects the horizontal shift along the frequency axis (time scale), while b_c reflects the vertical shift along the modulus axis (network density). This method eliminates the ambiguity often associated with purely visual shifting. The procedure is schematically illustrated in Figure 4, where the displacement of the crossover point directly visualizes the physical meaning of the shift factors.

3.4 | Superposition and Zero-Shear Viscosity

Using the experimentally derived shift factors, the storage and loss moduli of the diluted samples are superposed onto the reference melt curve via:

$$G'(\omega,\phi)b_c^{-1} = G'\left(a_c\omega,1\right) \quad \text{and} \quad G''(\omega,\phi)b_c^{-1} = G''\left(a_c\omega,1\right) \tag{3}$$

Furthermore, the zero-shear viscosity η_0, which represents the product of the elastic modulus scale and the characteristic relaxation time ($\eta_0 \sim G_N^0 \cdot \tau_d$), relates to the shift factors as follows:

$$\eta_0(\phi) = \eta_0(1)a_c b_c \tag{4}$$

This relationship facilitates the construction of a master viscosity curve covering an extended range of shear rates that would otherwise remain inaccessible due to experimental limitations.

4 | Results and Discussion

Unless noted otherwise, all kinetic fits and regression metrics discussed herein were computed using the mathematical framework outlined in Appendix A.

4.1 | Sorption Tests

To establish a uniform baseline across all samples, gravimetric sorption tests were conducted under identical processing conditions. Following exposure, the specimens were weighed to determine the final gravimetric diluent mass fractions, as compiled in Table 4.

The sub-saturation mass fractions exhibit a consistent, monotonic trend with hydrocarbon chain length for *n*-decane, *n*-dodecane, and *n*-tetradecane, with PE-LLD systematically accommodating more diluent than PE-HD (Table 4). Since sorption is conducted at 150°C, both polymers are fully molten. This single-phase isotropic state is corroborated by subsequent DSC measurements revealing a pronounced diluent-induced melting point depression that shifts T_m below the sorption temperature. To evaluate the thermodynamic

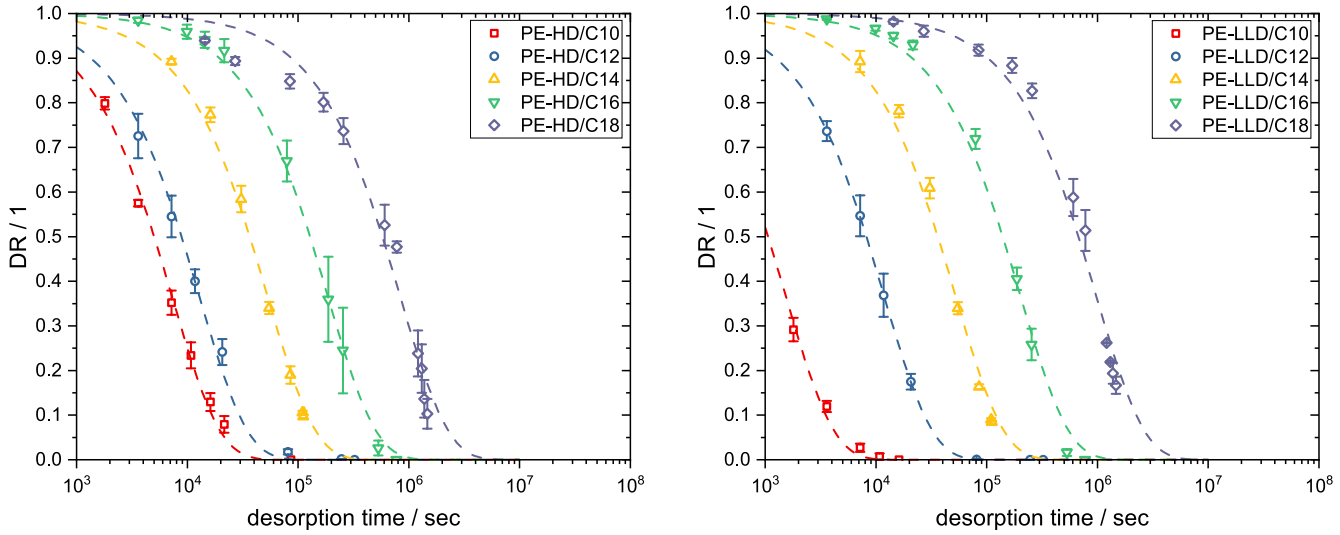

FIGURE 5 | Desorption kinetics of (a) PE-HD and (b) PE-LLD with various *n*-alkanes. Dashed lines: Model fits; symbols: Experimental data (error bars are the corresponding standard deviations). [Color figure can be viewed at wileyonlinelibrary.com]

affinity, Hildebrand solubility parameters (δ) were compiled from literature (Table 3) [27]. The close proximity between the bulk polymer ($\delta_{PE} \approx 16.8\,MPa^{1/2}$) and the linear alkanes ($\delta \approx 15.8 - 16.5\,MPa^{1/2}$, yielding $\Delta\delta \leq 1.0\,MPa^{1/2}$) confirms excellent chemical compatibility, ensuring that mass transport operates via high-rate liquid–liquid Fickian molecular diffusion rather than restricted solid-state swelling. Consequently, the higher accommodation capacity of PE-LLD stems from its short-chain branching architecture, which enhances the melt-state specific free volume and thermodynamic interaction parameters compared to the strictly linear backbone of PE-HD [18]. This guarantees that both sorption and rheological testing reside entirely within a homogeneous macromolecular solution regime, free from crystalline interfaces or concentration gradients.

In contrast, the *n*-hexadecane (C_{16}) system yielded an anomalous concentration drop and an elevated standard deviation. As flagged in Table 4, subsequent frequency sweeps showed severe deviations in shifting and poor reproducibility. Suspecting a localized batch contamination, the *n*-hexadecane dataset was entirely omitted from the subsequent modeling and master curve optimization to preserve the comparative rigor of the superposition framework.

The chosen sorption duration of 30 min represents a deliberate compromise between diffusion kinetics and material stability. While extended holding periods would drive the system closer to absolute thermodynamic equilibrium, prolonged residence times at 150°C pose a severe risk of thermal-oxidative degradation. At the high diluent mass fractions investigated (up to 65%), the internal antioxidant stabilization packages of the commercial polyethylenes are substantially diluted, leaving the backbone chains vulnerable to crosslinking or chain scission. However, the successful collapse of independent frequency sweeps onto the smooth master curves (Figure 9) empirically confirms that 30 min provides an optimal processing window: it ensures macroscopic concentration homogeneity while successfully suppressing thermal degradation artifacts.

4.2 | Desorption Tests

To achieve concentrations below saturation, desorption experiments were conducted in a convection oven at 80°C. Mass-loss curves were recorded by intermittent weighing, and subsequently fitted with simplified desorption models. For each system, an empirical relation was determined.

In a first approximation, desorption was described by first-order kinetics with a single fitting parameter: the desorption constant $k(N)$, which depends on the chain length N. The exponential decay function is:

$$DR(N,t) = \exp(-k(N)t), \tag{5}$$

where $DR(t)$, the dilution ratio, is defined as:

$$DR(t) = \frac{m(t) - m_\infty}{m_0}, \tag{6}$$

with m_0 the initial mass and m_∞ the polymer mass after complete desorption.

Figure 5 shows the experimental curves and corresponding fits. The simplified model described most systems well, with greater deviations for PE-HD/C12. When $k(N)$ is plotted versus alkane chain length, a quasi-linear dependency emerges, as shown in Figure 6.

The fitted parameters and performance metrics are summarized in Table 5, and the global model accuracy is shown in Figure 7.

It is important to analyze the distinct kinetic divergence observed for the *n*-decane (C_{10}) system in Figure 6, where the desorption rate in PE-HD is systematically lower than in PE-LLD, while the longer-chain homologs exhibit nearly identical drying rates across both matrices. This behavior is fundamentally rooted in

the semicrystalline morphology of the polymers at the drying temperature of 80°C. Unlike the subsequent rheological sweeps, 80°C resides well below the crystalline melting peaks, meaning the impermeable crystalline lamellae act as physical obstacles that induce geometric tortuosity. Because PE-HD possesses a significantly higher crystallinity (~ 69.6%) than PE-LLD (~ 39.5%), the transport path for the highly volatile and compact C_{10} molecules is severely restricted by tortuosity barriers in the high-density PE. For longer diluents (C_{14}–C_{18}), their larger molecular size renders bulk diffusion within the amorphous channels inherently sluggish, which effectively masks this structural tortuosity contrast.

Crucially, when the homogenized solutions are heated to the characterization temperatures (150°C and 180°C) for rheometry, these crystalline structures collapse completely into a fully amorphous single phase, eliminating any residual crystalline remnants. However, the localized concentration boundary layers established during the semicrystalline desorption stage introduce a minor systematic offset in the initial gravimetric mass fraction tracking, which directly accounts for the slight downward deviation observed in the vertical shift factor (b_c) baseline for the C_{10} systems in Figure 11.

Overall, most systems followed first-order desorption kinetics, which suggests concentration-independent drying rates. Deviations were observed, but given the objective of estimating drying times, the simplified model was considered sufficient. More detailed analyses could employ temperature-programmed desorption (TPD) combined with Redhead analysis [36, 37] or other models like the Verma model [38]. Future studies should also consider potential extraction of amorphous polymer fractions [20].

4.3 | Rheometry of Diluted Polyethylene

The rheological behavior of diluted polyethylene melts was systematically investigated using parallel-plate rheometry. As anticipated, the incorporation of *n*-alkanes induced a pronounced reduction in melt viscosity [19, 39]. To mitigate the risk of diluent volatilization, all experiments were conducted at the lowest feasible temperatures: 180°C for PE-HD and 150°C for PE-LLD.

The dilution effect was characterized by distinct vertical and horizontal shifts of the viscosity curve relative to the neat polymer, a trend consistently observed across all investigated diluents. Figure 8 illustrates this behavior for the exemplary case of *n*-dodecane; corresponding data for the remaining systems are provided in Figures A1 and A2.

Given that low-molecular-weight alkanes may act as external lubricants at the polymer–wall interface, the potential occurrence

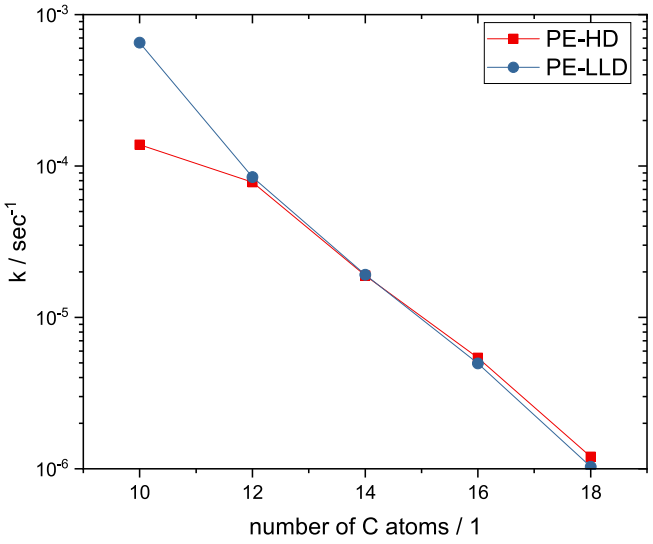

FIGURE 6 | Desorption rate constant k as a function of *n*-alkane chain length N. [Color figure can be viewed at wileyonlinelibrary.com]

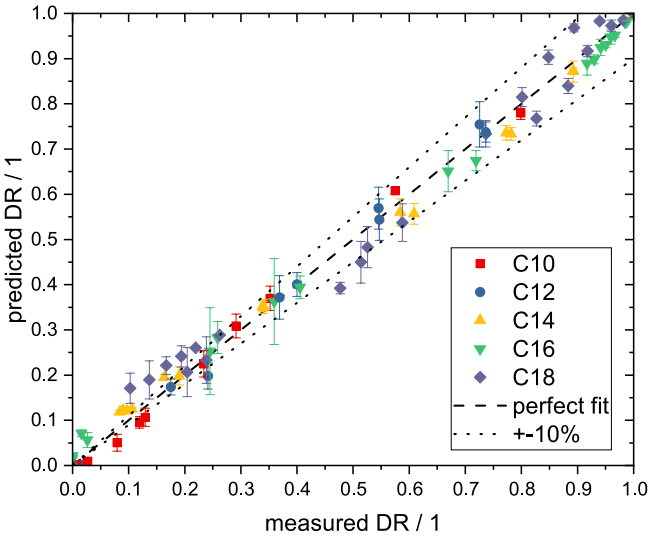

FIGURE 7 | Scatter plot of experimentally determined and predicted dilution ratios *DR*. Colors indicate diluents. [Color figure can be viewed at wileyonlinelibrary.com]

TABLE 5 | Desorption kinetic parameters and performance metrics.

	PE-HD			PE-LLD		
Diluent	k	R^2	**MRE**	k	R^2	**MRE**
C10	1.4E-4	0.997	0.101	6.5E-4	0.999	0.360
C12	7.8E-5	0.997	0.310	8.5E-5	0.999	0.190
C14	1.9E-5	0.998	0.077	1.9E-5	0.995	0.143
C16	5.4E-6	0.999	0.142	5.0E-6	0.997	0.408
C18	1.2E-6	0.981	0.130	1.0E-6	0.987	0.101

of wall slip was rigorously scrutinized. This was evaluated by performing measurements at varying gap heights in the parallel-plate setup. The invariance of the apparent viscosity with decreasing gap height substantiated the absence of wall slip under the applied conditions. Verifying this condition was essential, as the presence of slip would have necessitated complex shear-rate corrections, as described by Yoshimura and Prud'homme [40].

To consolidate the rheological data, the viscosity curves of the diluted samples were shifted using the corresponding horizontal a_c and vertical b_c shift factors, aligning them with the reference curve of the undiluted PE-HD and PE-LLD. As demonstrated in Figure 9, the resulting data points collapse onto a single, continuous master curve, confirming the validity of the time–concentration superposition principle for these systems.

Following the successful superposition, the influence of diluent concentration and diluent type on the shift factors a_c and b_c was systematically analyzed, as presented in Figure 10 and latter Figure 11.

As observed in Figure 10, the horizontal shift factor a_c decreases systematically and monotonically with increasing diluent chain length across the entire homologous series (C10 through C18), for both PE-HD and PE-LLD. This trend is opposite to the naive prediction of chain-end free-volume theory, which would predict

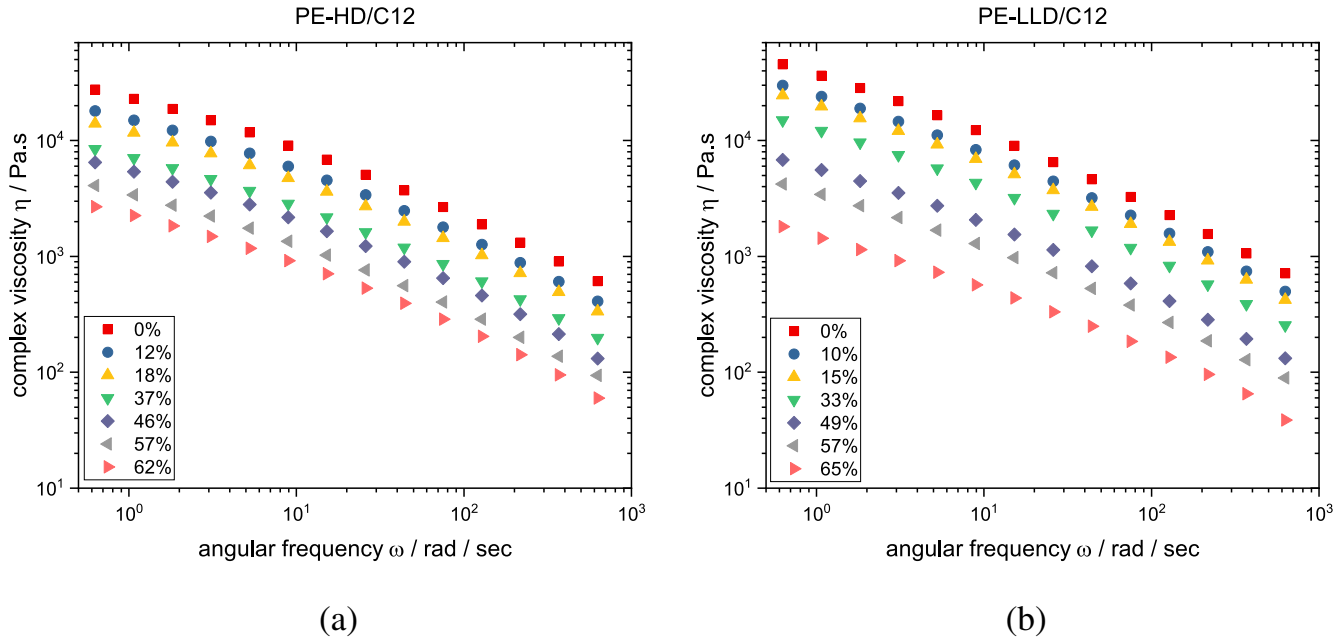

FIGURE 8 | Shear viscosity as a function of shear rate for systems diluted with *n*-dodecane: (a) PE-HD at 180°C, and (b) PE-LLD at 150°C. [Color figure can be viewed at wileyonlinelibrary.com]

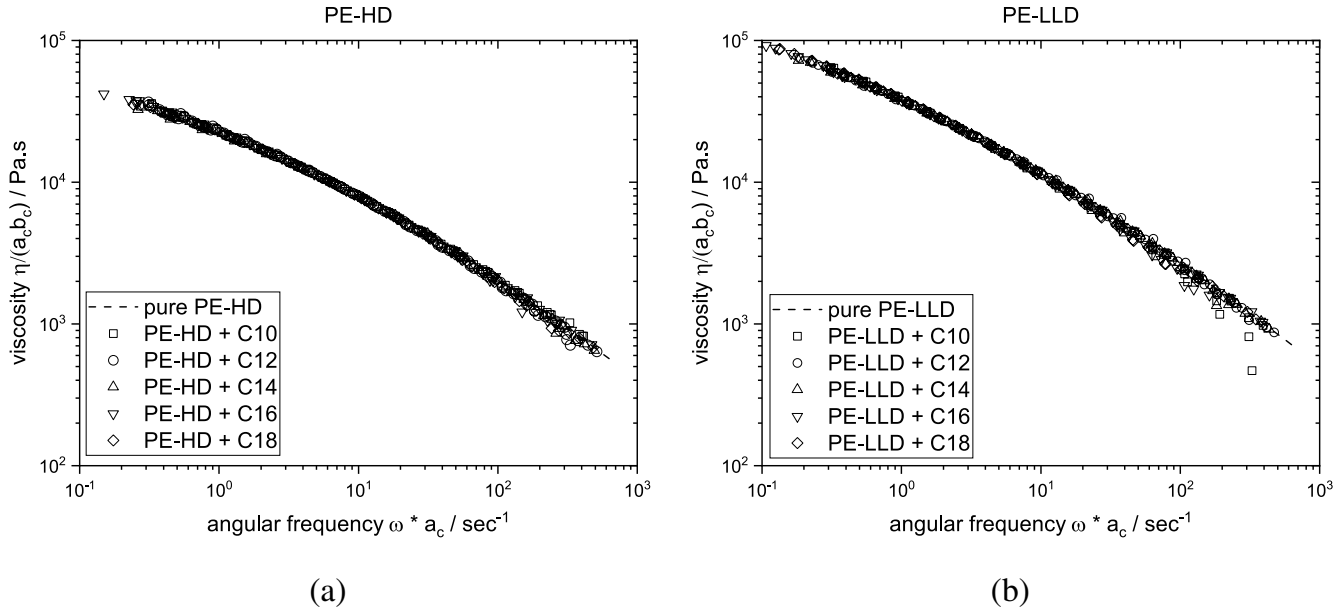

FIGURE 9 | Unified master curves obtained via time–concentration superposition for: (a) PE-HD at 180°C, and (b) PE-LLD at 150°C.

a stronger a_c shift for the shorter, more numerous-chain-end diluents. Because this reversal is observed consistently across the full alkane series, including C14 and C18, whose boiling points lie far above both characterization temperatures, an evaporative or thermal artifact can be ruled out as the primary cause; a volatility-driven effect would be expected to selectively affect only the shortest, most volatile diluents (C10, C12), not the series as a whole.

We instead attribute this systematic trend to a genuine, chain-length-dependent difference in how effectively each diluent couples to the polymer's segmental and reptational dynamics. While all *n*-alkanes contribute to entanglement dilution in proportion to their weight fraction (governing b_c, Section III A), their effectiveness at accelerating the local monomeric friction and disengagement dynamics that govern a_c may depend on the diluent's own chain length relative to the entanglement spacing. Shorter, highly mobile diluent molecules (e.g., C10) may diffuse through the free volume without efficiently coupling to segmental relaxation of the polymer backbone, whereas longer oligomeric diluents (e.g., C18), being closer in size to a Rouse segment, may couple more effectively to local chain motion and thus produce a larger acceleration of τ_d per unit diluent mass fraction. We note that this interpretation is consistent with our data but has not been independently verified here, and we propose it as a hypothesis for future investigation rather than an established mechanism.

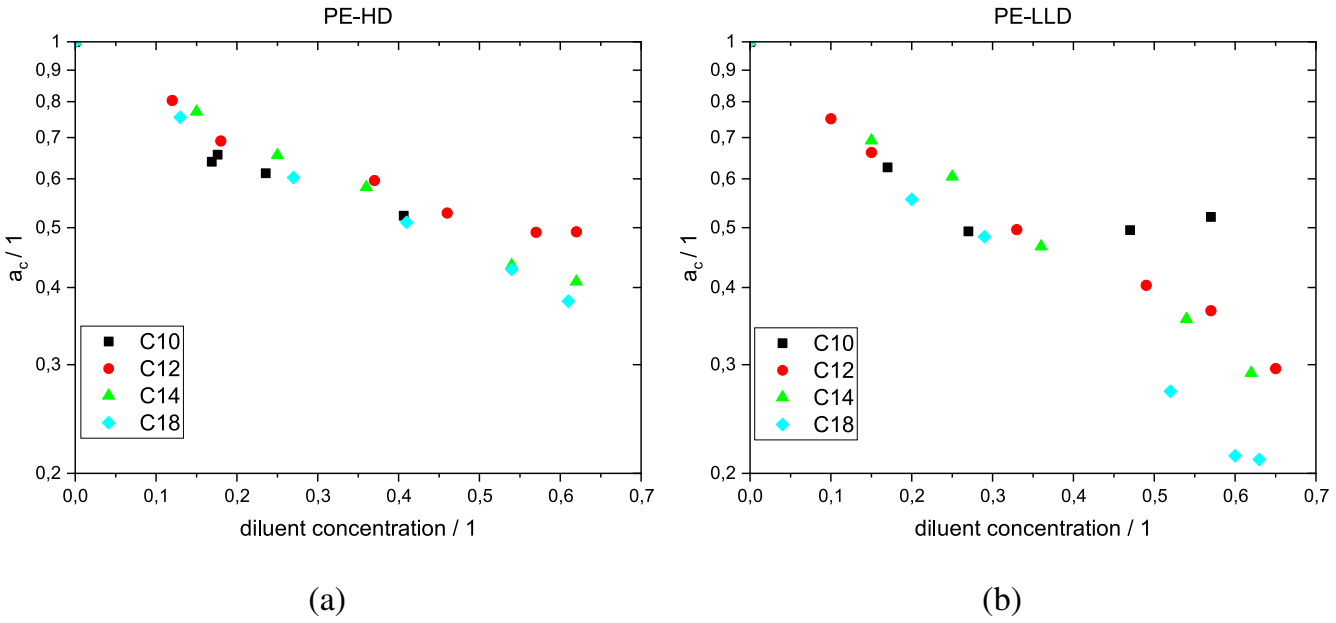

FIGURE 10 | Concentration dependence of the horizontal shift factor a_c for: (a) PE-HD, and (b) PE-LLD. [Color figure can be viewed at wileyonlinelibrary.com]

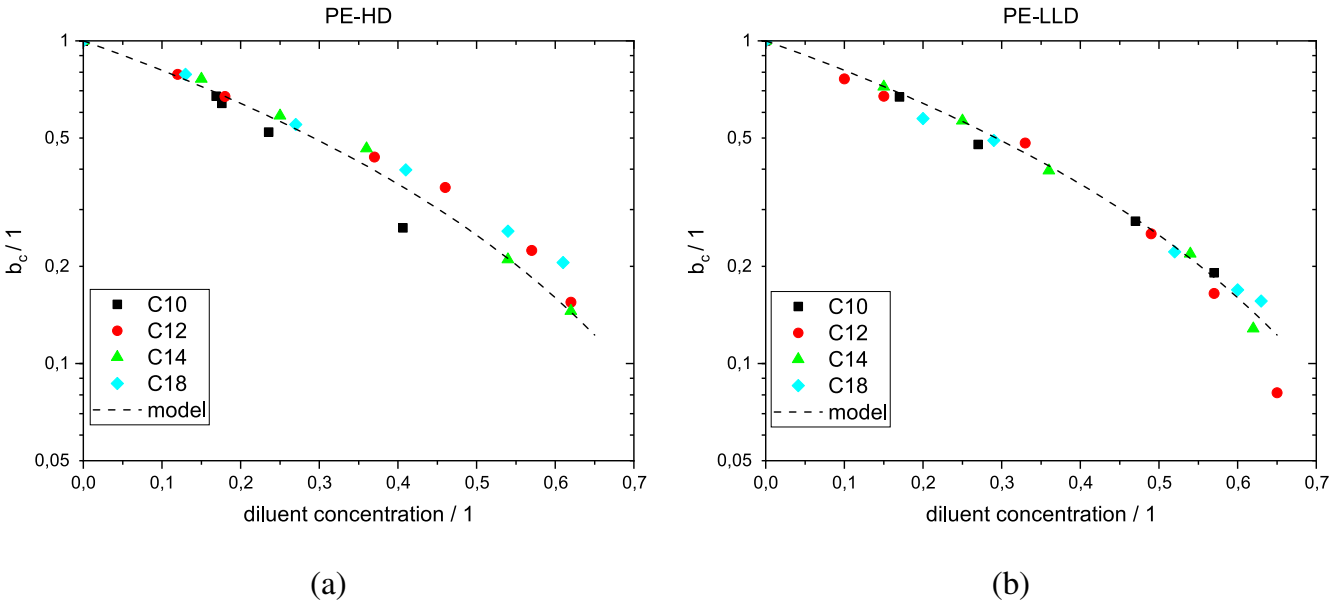

FIGURE 11 | Concentration dependence of the vertical shift factor b_c for: (a) PE-HD, and (b) PE-LLD. The dotted line represents the model prediction according to Equation (7). [Color figure can be viewed at wileyonlinelibrary.com]

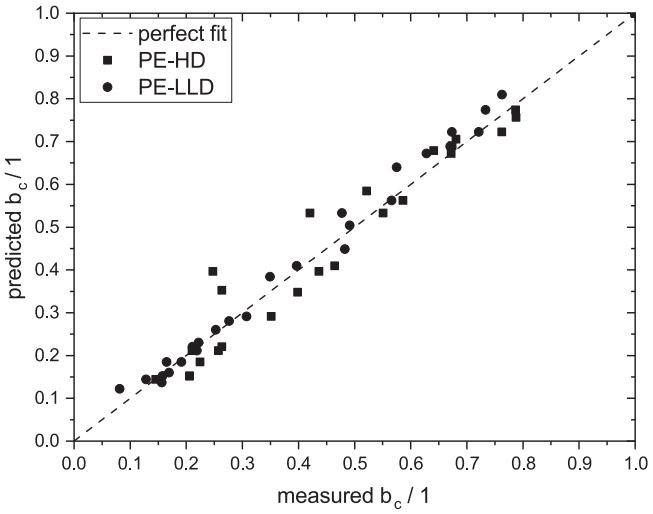

FIGURE 12 | Scatter plot comparing the experimentally determined vertical shift factors b_c with the model predictions according to Equation (7) for PE-HD and PE-LLD.

To rigorously quantify the vertical shift behavior, the modulus shift factor b_c was modeled utilizing the theoretical framework established by Schausberger and Ahrer [10]. This approach attributes the reduction in the plateau modulus primarily to the dilution of the entanglement network, a relationship mathematically expressed as:

$$b_c = w_P^2, \tag{7}$$

where w_P denotes the weight fraction of the polymer in the diluted system. The applicability of this model is demonstrated in Figure 11, where the experimentally derived shift factors are plotted alongside the theoretical prediction curve. A systematic decrease in b_c with increasing diluent concentration is observed for both PE-HD and PE-LLD, showing excellent agreement with the quadratic dilution law.

To further assess the predictive capability, the calculated values were compared against the experimentally derived shift factors in a scatter plot. Figure 12 illustrates the correspondence between the predicted and experimental b_c values.

The predictive accuracy of the model is substantiated by the quantitative performance metrics calculated for both materials. For PE-HD, the analysis yielded a mean relative error (MRE) of 0.109 and a coefficient of determination (R^2) of 0.970. The PE-LLD system demonstrated an even higher degree of correlation, characterized by an MRE of 0.064 and an R^2 of 0.994. These results confirm that the squared-concentration dependence provides a robust description for both polyethylene types within the investigated concentration range.

5 | Conclusion

This study systematically elucidated the influence of low-molecular-weight *n*-alkane diluents on the linear viscoelastic properties of polyethylene melts. By integrating gravimetric sorption analysis with oscillatory shear rheometry, a robust methodological framework was established to generate polymer–diluent solutions with defined concentration levels and to rigorously quantify the resultant modification of melt rheology.

Gravimetric analysis substantiated that the gravimetric diluent mass fraction is governed by the macromolecular architecture, with the short-chain branched PE-LLD demonstrating a markedly higher melt-state sorption capacity than the linear PE-HD due to an enhanced specific free volume. Furthermore, controlled desorption allowed for the precise and reproducible adjustment of sub-saturation concentrations. The drying kinetics were well approximated by a first-order exponential model, illustrating a systematic decrease in rate constants with increasing alkane chain length.

Rheological characterization revealed a pronounced reduction in melt viscosity upon dilution. This phenomenon was successfully analyzed using the Time–Concentration Superposition (TCS) principle. The application of horizontal (a_c) and vertical (b_c) shift factors facilitated the consolidation of viscoelastic data across various concentrations into unified master curves, confirming the validity of the superposition principle for these systems. Notably, the experimentally determined vertical shift factor b_c was found to follow a quadratic concentration dependence ($b_c \approx w_P^2$). This result aligns perfectly with the theoretical framework of entanglement network dilution as postulated by Schausberger and Ahrer, validating the physical basis of the observed modulus reduction.

In contrast, the horizontal shift factor a_c exhibited a clear, monotonic dependence on diluent chain length across the entire homologous series (C10 through C18) for both polymers, but with a sign opposite to the naive prediction of chain-end free-volume theory: longer diluents produced a systematically larger acceleration of the relaxation time than shorter, more numerous-chain-end homologs. Because this trend was observed consistently across the full series, including the least volatile diluents, whose boiling points lie far above the characterization temperatures, it cannot be attributed to an evaporative or thermal artifact, which would be expected to selectively affect only the most volatile, shortest-chain diluents. We instead attribute this behavior to a genuine, chain-length-dependent difference in how effectively each diluent couples to the segmental and reptational dynamics of the polymer backbone, a mechanism distinct from the pure network-dilution effect captured by b_c. We propose this coupling-based interpretation as a hypothesis motivating future work, (e.g., systematically varying diluent chain length relative to the entanglement molecular weight M_e), rather than as an established mechanism.

This study opens a clear avenue for future fundamental investigations into advanced dilution regimes. Should the chain-length dependence of a_c be resolved further, the present framework could be extended to model a_c and b_c jointly across a substantially broader concentration range. Our companion studies have already demonstrated feasibility in this direction, characterizing diluent mass fractions up to approximately 40% in polyethylene melts [41] and, using pressurized slit-die rheometry, up to approximately 90% diluent content [34]. At such elevated dilution levels, a transition from tube-confined reptation to unentangled Rouse dynamics is eventually expected, the onset of which will depend on the specific polymer–diluent pair investigated.

While the present work was instrumentally restricted to the highly concentrated domain ($w_P \geq 0.35$) where tube-confined reptation remains strictly dominant, systematically pushing the polymer concentration further downward represents a highly compelling next step. Extending the characterization into ultra-dilute regimes ($w_P < 0.30$)—ideally utilizing specialized equipment—would allow for the explicit visualization of the network disassembly. Capturing the threshold where the rubbery plateau modulus (G_N^0) vanishes would enable a comprehensive mapping of the structural transition from entangled reptation to unentangled Rouse dynamics, thereby resolving the theoretically predicted multi-regime concentration scaling laws across the entire polyolefin-solvent space.

In summary, the presented methodology offers a reproducible approach for characterizing viscosity reduction in polyethylene–alkane systems. By validating the quadratic scaling of the plateau modulus, this work provides a solid predictive basis for the design and optimization of polymer processing operations that rely on diluent-assisted rheology modification, such as foam extrusion and devolatilization.

Author Contributions

Ernst Georg Viehböck: conceptualization, investigation, writing – original draft, methodology, validation, visualization, writing – review and editing, formal analysis, data curation, software, supervision. **Georg Gschwendner:** investigation, writing – review and editing, methodology, conceptualization, validation. **Gunnar Spiegel:** supervision, conceptualization, methodology, writing – review and editing, project administration. **Dario Pindrić:** investigation, conceptualization, methodology, writing – review and editing, supervision. **Alexander Hammer:** writing – review and editing, supervision, conceptualization, methodology, formal analysis. **Christian Paulik:** supervision, resources, project administration, funding acquisition, writing – review and editing, conceptualization, methodology. **Gerald Berger-Weber:** resources, funding acquisition, writing – review and editing, project administration, supervision.

Acknowledgments

During the preparation of this work the authors used Chat GPT-5 and Gemini 3 Pro in order to increase readability and image generation. After using this tool, the authors reviewed and edited the content as needed and employed a professional editor and take full responsibility for the content of the published article. Open Access funding provided by Johannes Kepler Universitat Linz.

Funding

The authors acknowledge support through the FTI initiative circular economy "circPLAST-mr", funded by the BMIMI (Austrian federal ministry for innovation, mobility and infrastructure, grant no. 889843) and the FFG (Austrian Research Promotion Agency). This work was conducted as part of the COMET Center CHASE, funded within the COMET—Competence Centers for Excellent Technologies programme by the BMIMI, the BMWET (Austrian federal ministry for economy, energy and tourism) and the Federal Provinces of Upper Austria and Vienna. The COMET programme is managed by the FFG. This article was funded by the Johannes Kepler Open Access Publishing Fund and the federal state Upper Austria.

Conflicts of Interest

The authors declare no conflicts of interest.

Data Availability Statement

The data that support the findings of this study are available from the corresponding author upon reasonable request.

References

1. C. G. Gogos and Z. Tadmor, *Principles of Polymer Processing* (John Wiley & Sons, 1979).

2. S.-T. Lee and C. B. Park, eds., "Foam Extrusion: Principles and Practice," in *Polymeric Foams Series* (CRC Press, 2014).

3. L. J. Gerhardt, A. Garg, C. W. Manke, and E. Gulari, "Concentration-Dependent Viscoelastic Scaling Models for Polydimethysiloxane Melts With Dissolved Carbon Dioxide," *Journal of Polymer Science Part B: Polymer Physics* 36 (1998): 1911–1918.

4. J. R. Royer, Y. J. Gay, J. M. Desimone, and S. A. Khan, "High-Pressure Rheology of Polystyrene Melts Plasticized With CO_2: Experimental Measurement and Predictive Scaling Relationships," *Journal of Polymer Science Part B: Polymer Physics* 38 (2000): 3168–3180.

5. X. Qin, M. Thompson, A. Hrymak, and A. Torres, "Rheology Studies of Polyethylene/Chemical Blowing Agent Solutions Within an Injection Molding Machine," *Polymer Engineering & Science* 45 (2005): 1108–1118.

6. T. Schaible and C. Bonten, "In-Line Measurement and Modeling of Temperature, Pressure, and Blowing Agent Dependent Viscosity of Polymer Melts," *Applied Rheology* 32 (2022): 69–82.

7. C. D. Han, *Rheology and Processing of Polymeric Materials* (Oxford University Press, 2007).

8. A. Schausberger, H. Knoglinger, and H. Janeschitz-Kriegl, "The Role of Short Chain Molecules for the Rheology of Polystyrene Melts. II. Linear Viscoelastic Properties," *Rheologica Acta* 26 (1987): 468–473.

9. H. Knoglinger, A. Schausberger, and H. Janeschitz-Kriegl, "The Role of Short Chain Molecules for the Rheology of Polystyrene Melts. I. Molar Mass Dependent Shift Factors," *Rheologica Acta* 26 (1987): 460–467.

10. A. Schausberger and I. V. Ahrer, "On the Time-Concentration Superposition of the Linear Viscoelastic Properties of Plasticized Polystyrene Melts Using the Free Volume Concept," *Macromolecular Chemistry and Physics* 196 (1995): 2161–2172.

11. E. Kastner, "Zeit-Konzentration-Superposition am Beispiel konzentrierter Polyethylenlösungen," 1996.

12. T. M. Aminabhavi and H. G. Naik, "Sorption/Desorption, Diffusion, Permeation and Swelling of High Density Polyethylene Geomembrane in the Presence of Hazardous Organic Liquids," *Journal of Hazardous Materials B* 64, no. 3 (1998): 251–262.

13. T. De Loos, L. De Graaf, and J. De Swaan Arons, "Liquid–Liquid Phase Separation in Linear Low Density Polyethylene–Solvent Systems," *Fluid Phase Equilibria* 117 (1996): 40–47.

14. F. Hamada, K. Fujisawa, and A. Nakajima, "Lower Critical Solution Temperature in Linear Polyethylene–n-Alkane Systems," *Polymer Journal* 4 (1973): 316–322.

15. J. L. Budzien, J. D. McCoy, D. H. Weinkauf, R. A. LaViolette, and E. S. Peterson, "Solubility of Gases in Amorphous Polyethylene," *Macromolecules* 31 (1998): 3368–3371.

16. P. Paricaud, A. Galindo, and G. Jackson, "Modeling the Cloud Curves and the Solubility of Gases in Amorphous and Semicrystalline Polyethylene With the SAFT-VR Approach and Flory Theory of Crystallization," *Industrial & Engineering Chemistry Research* 43 (2004): 6871–6889.

17. N. Schlotter and P. Furlan, "A Review of Small Molecule Diffusion in Polyolefins," *Polymer* 33 (1992): 3323–3342.

18. T. R. Ehrmann, "Modeling the Isothermal Thermogravimetric Behavior of Polymer-Volatile Systems," 2024.

19. G. Gschwendner, "Viscoelastic Behavior of Diluted Polyethylene," 2024.

20. A. B. Mrad, N. Sheibat-Othman, A. P. A. Amorim, R. L. Do Rosario, and T. F. L. McKenna, "Polyethylene Slurries: Swelling and Solubility," *Macromolecular Reaction Engineering* 17 (2023): 2300020.

21. F. Klaiber, I. D. L. Gomez, T. A. Osswald, and L. S. Turng, "Development of a High-Pressure Slit Rheometer," in *Society of Plastics Engineers Annual Technical Conference* (Society of Plastics Engineers, 2006), 2320–2324.

22. T. A. Osswald and N. S. Rudolph, *Polymer Rheology: Fundamentals and Applications* (Hanser Publications, 2015).

23. R. Gendron and A. Correa, "The Use of On-Line Rheometry to Characterize Polymer Melts Containing Physical Blowing Agents*," *Cellular Polymers* 17 (1998): 93–113.

24. Y. Sato, M. Yurugi, K. Fujiwara, S. Takishima, and H. Masuoka, "Solubilities of Carbon Dioxide and Nitrogen in Polystyrene Under High Temperature and Pressure," *Fluid Phase Equilibria* 125 (1996): 129–138.

25. Y. Kong and J. Hay, "The Measurement of the Crystallinity of Polymers by DSC," *Polymer* 43 (2002): 3873–3878.

26. G. W. Gokel and J. A. Dean, "Dean's Handbook of Organic Chemistry," in *McGraw-Hill Handbooks*, 2nd ed. (McGraw-Hill, 2004).

27. A. F. Barton, *CRC Handbook of Solubility Parameters and Other Cohesion Parameters: Second Edition*, 2nd ed. (Routledge, 2017).

28. K. V. Pochivalov, T. N. Lebedeva, A. N. Ilyasova, A. V. Basko, and Y. V. Kudryavtsev, "A New Look at the Semicrystalline Polymer—Liquid Systems: Phase Diagrams Low-Density Polyethylene—N-Alkanes," *Fluid Phase Equilibria* 471 (2018): 1–7.

29. T. Mezger, "Das Rheologie Handbuch: 5., überarbeitete Auflage, FARBE UND LACK // BIBLIOTHEK," 2016.

30. J. D. Ferry, *Viscoelastic Properties of Polymers* (John Wiley & Sons, 1980).

31. W. Graessley, "Polymer Chain Dimensions and the Dependence of Viscoelastic Properties on Concentration, Molecular Weight and Solvent Power," *Polymer* 21 (1980): 258–262.

32. M. Doi and S. F. Edwards, "The Theory of Polymer Dynamics," in *International Series of Monographs on Physics* (Clarendon Press, 1994).

33. R. H. Colby, L. J. Fetters, W. G. Funk, and W. W. Graessley, "Effects of Concentration and Thermodynamic Interaction on the Viscoelastic Properties of Polymer Solutions," *Macromolecules* 24 (1991): 3873–3882.

34. J. Krug, E. G. Viehböck, A. Hammer, et al., "Rheological Characterization and Multi-Regime Viscosity Modeling of Diluted Polyethylene Mixtures," *Polymer Engineering & Science* 66 (2026): 4913–4925, https://doi.org/10.1002/pen.70545.

35. F. N. Kelley and F. Bueche, "Viscosity and Glass Temperature Relations for Polymer-Diluent Systems," *Journal of Polymer Science* 50 (1961): 549–556.

36. P. Redhead, "Thermal Desorption of Gases," *Vacuum* 12 (1962): 203–211.

37. K. R. Paserba and A. J. Gellman, "Effects of Conformational Isomerism on the Desorption Kinetics of *n*-Alkanes From Graphite," *Journal of Chemical Physics* 115 (2001): 6737–6751.

38. E. G. Viehböck, T. Ehrmann, G. R. Berger-Weber, A. Hammer, M. Kirchmayr, and C. Paulik, "Modeling the Drying Kinetics of Polymer Volatile Systems Using Thermogravimetric Analysis Data," in *Proceedings of the Polymers, Composites, 3BsMaterials 2025 Joint International Conferences* (SETCOR Conferences and Events, 2025).

39. E. G. Viehböck, A. Hammer, M. Kirchmayr, C. Murnig, C. Paulik, and G. Berger-Weber, "Slit-Rheometry-Based Characterization of the Flow Behavior of Diluted Polymer Melts," *Journal of Rheology* 70 (2026): 35–45.

40. A. Yoshimura and R. K. Prud'homme, "Wall Slip Corrections for Couette and Parallel Disk Viscometers," *Journal of Rheology* 32 (1988): 53–67.

41. E. G. Viehböck, A. Hammer, M. Kirchmayr, C. Murnig, C. Paulik, and G. Berger-Weber, "Viscosity Reduction in Diluted Polyethylene Melts: A Comparative Study of Semiempirical, Viscoelastic, and Equation-of-State Modeling Frameworks," *Polymer Engineering & Science* 66, no. 5 (2026): 3386–3402, https://doi.org/10.1002/pen.70432.

Appendix A: Fitting Metrics

In order to fit all models evaluated using consistent performance criteria, several key metrics were defined and applied. The used fitting parameter is the weighted quadratic error WQE:

$$\mathrm{WQE} = \sum_{i=1}^{n} \frac{(x_i - y_i)^2}{x_i}, \tag{A1}$$

where x_i is the measured value, y_i is the predicted value, and n is the total number of data points.

Additionally, the coefficient of determination R^2 was calculated to assess how well the model explains the variance in the experimental data:

$$R^2 = 1 - \frac{\sum_{i=1}^{n} (x_i - y_i)^2}{\sum_{i=1}^{n} (x_i - \bar{x})^2}, \tag{A2}$$

where $\bar{x}$ is the mean of the measured values.

Finally, the mean relative error MRE was determined as:

$$\mathrm{MRE} = \frac{1}{n} \sum_{i=1}^{n} \left| \frac{x_i - y_i}{x_i} \right|. \tag{A3}$$

In all fitting tasks, the primary objective was to minimize the weighted quadratic error WQE, while the additional metrics R^2 and MRE were used solely for comparative performance assessment.

Appendix B: Additional Figures

Viscosity results for PE-HD and PE-LLD with the following diluents C10, C14, C16 and C18.

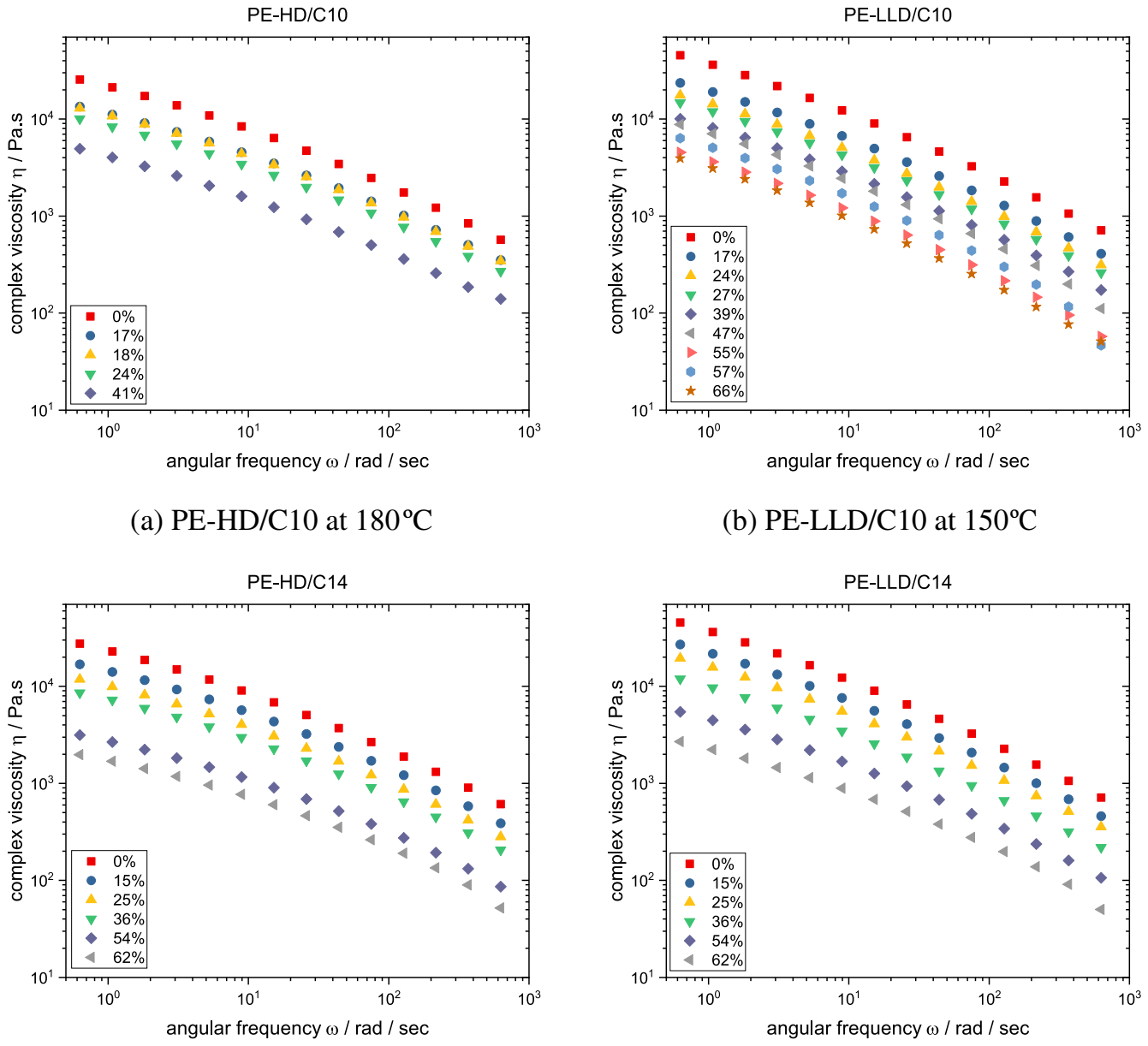

(a) PE-HD/C10 at 180°C

(b) PE-LLD/C10 at 150°C

(c) PE-HD/C14 at 180°C

(d) PE-LLD/C14 at 150°C

FIGURE A1 | Comparison of experimental viscosity data for some polymer–diluent systems studied. [Color figure can be viewed at wileyonlinelibrary.com]

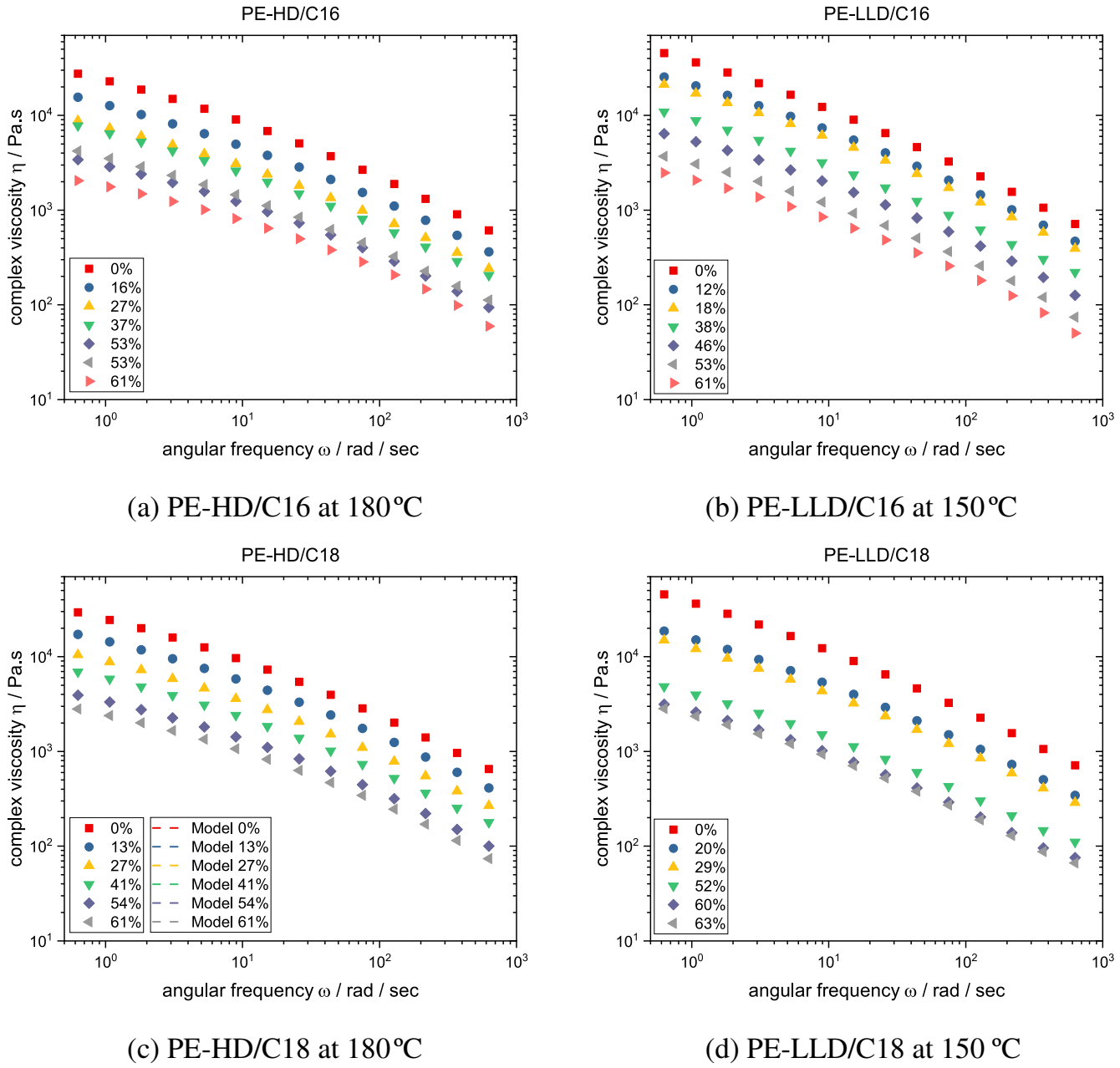

(a) PE-HD/C16 at 180°C

(b) PE-LLD/C16 at 150°C

(c) PE-HD/C18 at 180°C

(d) PE-LLD/C18 at 150 °C

FIGURE A2 | Comparison of experimental viscosity data for some polymer–diluent systems studied. [Color figure can be viewed at wileyonlinelibrary.com]